11

New Window on Optical Brain Imaging; Medical Development, Simulations and Applications

Chemseddine Mansouri[1] and Nasser H. Kashou[2,3,4]
[1]*CRAN UMR 7039 CNRS-UHP-INPL, Nancy University Vandoeuvre-les-Nancy,*
[2]*Department of Radiology, Children's Radiological Institute, Nationwide Children's Hospital*
[3]*Department of Radiology, Department of Ophthalmology, The Ohio State University Medical Center*
[4]*Department of Biomedical, Industrial and Human Factors Engineering, Wright State University,*
[1]*France*
[2,3,4]*USA*

1. Introduction

As telecommunications advances optical fiber technology, the costs decreases and signal quality increases. This trend is advantageous for the medical industry specifically for neurological applications and research. In general, the field of optics is based on light behavior. The addition of biological tissue interaction with this light introduces and extra factor. This opens up a field of modeling and optimization of the optical fibers based on scattering, absorption and paths traversed by these photons. This modeling includes simulation and signal reconstruction in order to quantify chromophore concentrations in biological tissue, in this case the human head.

Functional near-infrared spectroscopy (fNIRS) allows the ability to monitor brain activation by measuring changes in the concentration of oxy- and deoxy-hemoglobin (Hb) by their different spectra in the near-infrared range (Arridge 1995; Arridge and Lionheart 1998; Arridge and Schweiger 1995; Benaron et al. 2000; Benaron and Stevenson 1993; Brazy et al. 1985; Chance et al. 1998; Cope 1991; Cope and Delpy 1988; Everdell et al. 2005; Ferrari et al. 2004; Franceschini 2000, 2003; Gandjbakhche et al. 1994; Gratton et al. 1995, 1997; Gratton and Fabiani 2003; Greisen 2006; Hintz et al. 1998, 1999, 2001; Hoshi 2003; Jasdzewski et al. 2003; Kato et al. 1993; Kusaka et al. 2004; Meek et al. 1995, 1998; Miki et al. 2005; Obrig and Villringer 2003; Obrig et al. 2000; Plichta et al. 2006; Schroeter et al. 2004, 2006a, 2006b; Strangman et al. 2002, 2003; Taga et al. 2003; Toronov et al. 2000; Villringer and Chance 1997; Wilcox et al. 2005; Wolf et al. 2003; Wyatt et al. 1988; Xu et al. 2005). Functional imaging with NIR light is made possible in a spectrum window that exists within tissues in the 600–950 nm NIR region, in which photon transport is dominated by scattering rather than absorption. For more than two decades, the

single channel measurement technique of NIR spectroscopy has been successfully used to measure the haemodynamic response to brain activity in both adults and neonates (Ferrari et al. 2004; Hoshi 2003; Obrig et al. 2000). In a typical design the photon can have three possible paths: scattering, absorption or transmission. Its resolution is intrinsically limited by the diffusive nature of NIR light in tissue. More recent studies using the multi channel NIRS technique, NIR optical topography (OT), have improved spatial and temporal resolution in both adults (Kennan et al. 2002) and infants (Taga et al. 2003).

NIRS measurement accuracy can vary depending on the design of the detector head. Constant optode distance is crucial; if head circumference changes even by a fraction of a millimeter, the trends are significantly biased (Greisen 2006). This dependency has been shown in both experiments and simulation. A comprehensive study was performed on factors affecting the accuracy of NIR concentration calculations and found that the wavelength selection and optode placement to be important factors in reducing error (Strangman et al. 2003). A limitation of NIR is its low spatial resolution (Gandjbakhche et al. 1994). On the other hand compared to other imaging methods, optical approaches have an excellent temporal resolution (Pouratian et al. 2003; Villringer and Chance 1997) that enables analysis in the frequency domain.

In this chapter we hope to give a technological review of near-infrared light and systems, discuss optode design considerations including background on the fiber design as it relates to this field and finally touch on current trends and applications. For the latter, we will focus on diffusion theory and simulation of photon propagation using a head model. We will follow this with concluding remarks.

2. Technology review

2.1 Light-tissue interaction

Interaction between light and the biological system consists of the absorption of light by a molecular species and the redirection of incidental light over a range of angles due to refractive index mismatch in tissue microstructure, i.e. scattering. The energy change measured by absorption is defined by

$$\Delta E = hv = h(c/\lambda) \tag{1}$$

Where c is the speed of light, λ is the wavelength and *h* is Planck's constant 6.626 x 10-34 J S. From this we can derive a relationship between the absorption of chromophores and the wavelength of light. **Fig. 1** shows the absorption spectrum of two chromophores that are particularly critical for NIRS, oxy- and dexoy- hemoglobin. As will be seen later, the choice of wavelengths for different systems is dependent upon this. We highlight 690 and 830 nm because of the difference in absorption for oxy- and deoxy- hemoglobin. From this figure we also see a point where the absorptivity is the same for both, about 805 nm. It is advantageous to include this additional wavelength as a quality and validation check for instruments.

This property of tissue will have a direct effect on the light pathway and behavior which leads us into another fundamental equation/law known as the Beer Lambert Law, **Equation 2**.

This states that the attenuation of light (I) as it travels through an absorptive tissue is directly proportional to the product of the concentration of the chromophore ([C]) and the optical path length (L), **Fig. 2**.

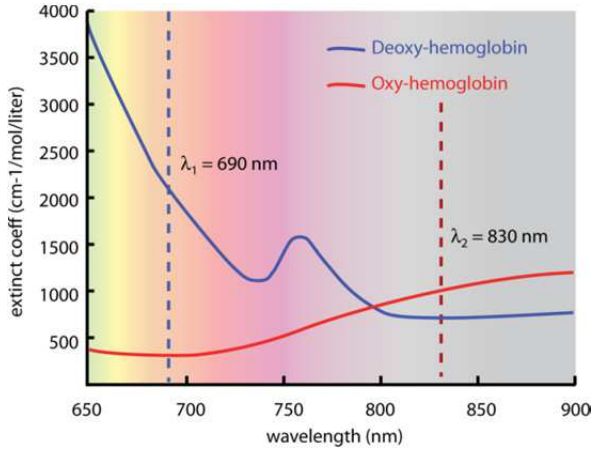

Fig. 1. Absorption spectrum of oxyhemoglobin (HbO) and deoxyhemoglobin (Hb) chromophores. Two or more wavelengths are needed to differentiate between these two chromophores, 690 and 830 nm are commonly used.

$$I = I_o \, e^{-\varepsilon[C]L} \tag{2}$$

Taking the log and inverting the output over input yields the attenuation

$$\mathrm{A} = \log\left(\frac{I_o}{I}\right) = \varepsilon[C]L \tag{3}$$

Again, note that absorption spectrum is dependent on the wavelength of light. Thus, a more appropriate formulation is

$$A_{\lambda_i} = \varepsilon_{\lambda_i}[C]L \tag{4}$$

Where λ_i is the i^{th} wavelength for the extinction coefficient (ε) based on **Fig. 1**. In the case of NIRS, two chromophores are unknown so we would need a minimum of two equations; meaning we need two wavelengths to find the solution, e.g. 690 and 830 nm. This formulation is common in pulse oximetry and follows the simple model shown in **Fig. 2(a),** where the light is transmitted at one end of the tissue and collected at the back end. For example, by placing a light source on our finger nail and a light detector directly opposite of that, on our finger. If we wanted to measure the light on the same side as our finger nail or concentration changes of a chromophore from more than one detector across a period of time then we will need to work with a slightly different equation as is discussed in the next subsection.

2.2 Near Infrared Light (NIR)

Near infrared light ranges from 600-950nm and is strongly absorbed by two chromophores, namely, oxyhemoglobin (HbO) and deoxyhemoglobin (Hb). As a result of this interaction, the modified Beer-Lambert Law (MBLL), seen in **Equation 5**, can be used to quantify changes in chromophore concentrations (Cope 1991; Cope and Delpy 1988).

$$\Delta\mathrm{OD} = -ln(I_{final}/I_{initial}) = \varepsilon\Delta\mathrm{CLB} \tag{5}$$

where $\Delta OD = OD_{final} - OD_{initial}$ is the change in optical density, I_{final} and $I_{initial}$ are the measured intensities before and after the concentration of the chromophores change, ΔC and replace I from **Equations 2 & 3**. L is the distance between incident light and detected light, ε is the extinction coefficient, and B is the differential path-length factor (DPF), **Fig. 2**. The general one chromophore equation can be further expanded for brain functional monitoring applications in which multiple wavelengths are used.

$$\Delta OD^{\lambda} = (\varepsilon^{\lambda}_{HbO}\Delta[HbO] + \varepsilon^{\lambda}_{Hb}\Delta[Hb])B^{\lambda}L \tag{6}$$

Where λ indicates particular wavelength. After rearranging the mathematical terms the concentration changes can now be computed by measuring the change in optical density at two different wavelengths as seen in **Equations 7 and 8**.

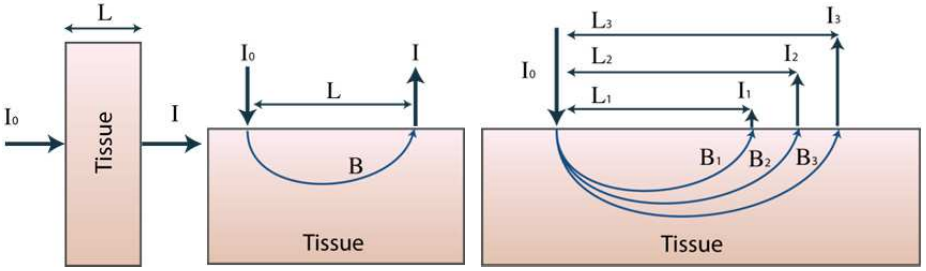

Fig. 2. (a) Light propagated through tissue (I_o) and transmitted at the output (I) traversing a distance L allows for chromophore concentration [C] calculations using Beer Lamberts Law. (b) Modified Beer Lamberts Law is used in this case as the photon traverses a path of distance (B). (c) Increasing the number of detectors and varying the distance allows for spatially resolved spectroscopy and several depths of penetration.This leads us to the modified Beer Lambert Law.

$$\Delta[Hb] = \frac{\left[\left(\varepsilon^{\lambda 2}{}_{HbO}\left(\Delta OD^{\lambda 1} / B^{\lambda 1}\right)\right) - \left(\varepsilon^{\lambda 1}{}_{HbO}\left(\Delta OD^{\lambda 2} / B^{\lambda 2}\right)\right)\right]}{\left[\left(\varepsilon^{\lambda 1}{}_{Hb}\varepsilon^{\lambda 2}{}_{HbO} - \varepsilon^{\lambda 2}{}_{Hb}\varepsilon^{\lambda 1}{}_{HbO}\right)L\right]} \tag{7}$$

$$\Delta[HbO] = \frac{\left[\left(\varepsilon^{\lambda 1}{}_{HbO}\left(\Delta OD^{\lambda 2} / B^{\lambda 2}\right)\right) - \left(\varepsilon^{\lambda 2}{}_{HbO}\left(\Delta OD^{\lambda 1} / B^{\lambda 1}\right)\right)\right]}{\left[\left(\varepsilon^{\lambda 1}{}_{Hb}\varepsilon^{\lambda 2}{}_{HbO} - \varepsilon^{\lambda 2}{}_{Hb}\varepsilon^{\lambda 1}{}_{HbO}\right)L\right]} \tag{8}$$

The basic process is now to shine two near infrared lights through the tissue, one which is more sensitive to oxyhemoglobin and the other to deoxyhemoglobin at two different time periods and take the difference of these concentrations. In this case all the other variables in **Equations 7 and 8** are defined by the design. This is possibly the simplest way to do these measurements. Next we will introduce the types of systems in use.

2.3 Experimental techniques

Time domain (TD), frequency domain (FD), and continuous-wave (CW) systems are currently being used to solve the above implementation of NIRS (Boas et al. 2002). For this

section we will discuss these three techniques separately and highlight the advantages and disadvantages of each.

2.3.1 Time domain

TD systems (Benaron and Stevenson 1993; Chance et al. 1988; Cubeddu et al. 1996; Grosenick et al. 1997; Hebden et al. 1997) introduce light impulses into tissue on the order of picoseconds which after passing through different layers such as skin, skull, cerebrospinal fluid (CSF), and brain become broadened and attenuated (Boas et al. 2002). The output of this pulse after being transmitted through the highly scattered medium is known as the temporal point spread function (TPSF)(Hebden et al. 1997), **Fig. 3**.

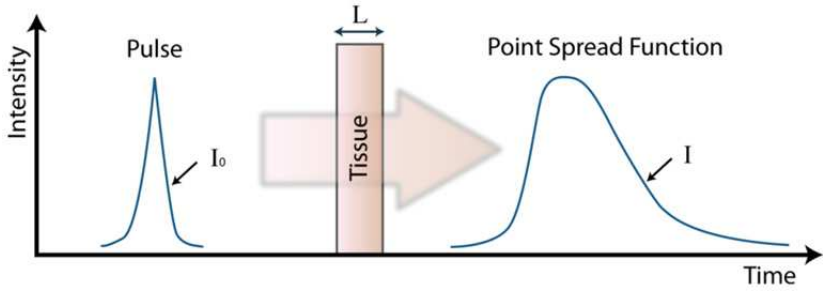

Fig. 3. In time domain systems an impulse (picoseconds) of light is sent through the tissue and the area of the point spread function is measured.

An advantage of TD systems over the other two is that theoretically it can obtain the highest spatial resolution and can accurately determine absorption and scattering (Boas et al. 2002). However, it has the disadvantage of lower temporal resolution as a direct result of trying to achieve an adequate signal to noise ratio, as well as the need to mechanically stabilize the instrument, the large dimensions and high cost of the necessary ultra fast lasers (Hebden et al. 1997).

2.3.2 Frequency domain

In FD systems, (Gratton et al. 1997; Jiang et al. 1995; Pogue et al. 1997; Pogue and Patterson 1994) the light source is continuously on but is amplitude modulated at frequencies on the order of tens to hundreds of megahertz, **Fig. 4**.

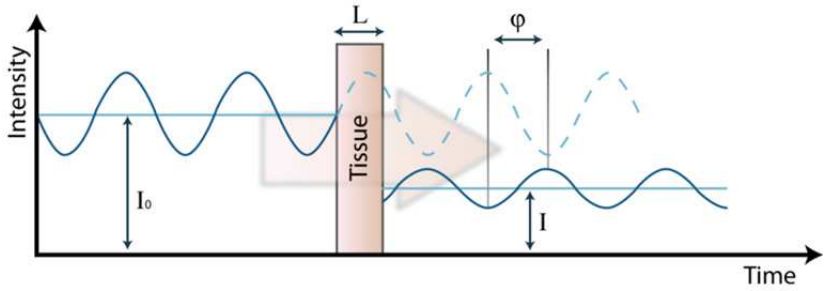

Fig. 4. In frequency domain systems a continuous intensity modulated source is sent through the tissue as a result and amplitude reduction and phase shifted signal is measured.

FD systems have the advantage of achieving higher temporal resolution than TD systems. One disadvantage is the noise in the measurements of scattering effects (Boas et al. 2002). Currently, FD is not as developed as the other two.

2.3.3 Continuous wave

In CW systems, (Maki et al. 1996; Nioka et al. 1997; Siegel et al. 1999) light sources emit light continuously at a constant amplitude or modulated frequencies not higher than a few tens of kilohertz (Boas et al. 2002). The most highly developed application of CW imaging technology is the study of hemodynamic and oxygenation changes in superficial tissues, and of the outer (cortical) regions of the brain; particularly using optical topography (Gibson et al. 2005). An advantage of CW systems over the other two is their cost. However, the main disadvantage is the inability to uniquely quantify the effects of light scattering and absorption (Arridge and Lionheart 1998). Other drawbacks are that intensity measurements are far more sensitive to the optical properties of tissues at or immediately below the surface than to the properties of localized regions deeper within the tissue (Gibson et al. 2005). This is due to the characteristic 'banana' shape **(seen in Fig. 2 (a) and (b))** of the volume of tissue over which the measurement is sensitive, which is narrow near the source and detector and very broad in the middle (Arridge 1995; Arridge and Schweiger 1995). Additionally, the detected intensity is highly dependent on surface coupling, meaning if an optical fiber is moved slightly or pressed more firmly on the skin, it can result in a significantly large change in measurement (Gibson et al. 2005). **Fig. 5** illustrates the CW system.

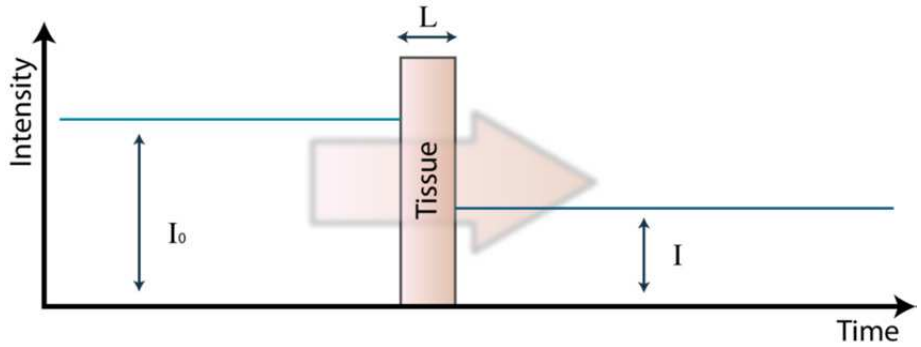

Fig. 5. In continuous domain systems, the light with constant is continuously emitted through the tissue and an attenuated signal is measured.

A more comprehensive discussion of these three systems will be beyond the scope of this chapter. A brief introduction was given so that a better understanding and ability to distinguish the protocols of current applications can be possible. Next we will discuss the optical fiber and configurations.

2.4 Optical fibers

Ideally, in transmitting light via optical fibers, we would achieve total internal reflection in the fiber as long as the incident angle is not too large, otherwise light will escape. Originally, bare fibers were used to transmit light. The limitation of using bare fibers is that the light guiding surface is exposed. For example, light could leak from finger prints, hence, fibers

currently consist of two layers; the core, for light transmittance and the cladding or barrier to keep the light from escaping, **Fig.6**. These layers have different indices of refraction.

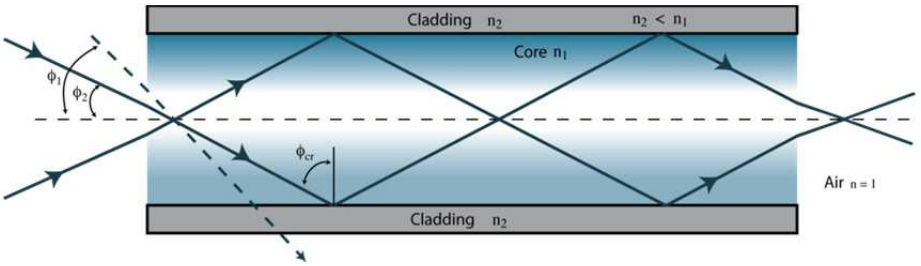

Fig. 6. Standard optical fiber light path. There is a slight refraction as the light enters the fiber from air. Cladding is used with a different index of refraction (n_2) to minimize light from escaping and entering. Based on the critical angle Φcr, the light either refracts into the cladding barrier or reflects back into the core as related to the angles of incidence Φ_1 andΦ_2.

The light is transmitted at incident angles which are given by Snell's law

$$n_1 \sin \Phi_1 = n_2 \sin \Phi_2 \tag{9}$$

where n and Φ are the refractive index and angle of incidence respectively. The light is refracted slightly inward as it passes from the air (n=1) to the optical fiber (n_1>n). Depending on the angle of incidence, the light may reflect back into the core or refract out into the cladding. The maximum angle of incidence allowable for some light to be refracted is called the critical angle (Φ_{cr}). Angles above this will result in total internal reflection when n_2<n_1.

$$\Phi_{cr} = \arcsin(\sin \Phi_2) \tag{10}$$

2.5 Optode considerations

In optimizing near infrared spectroscopy signals several considerations should be taken into account from the optode perspective. There are two types of materials that are used in designing the optical fibers; glass and plastic. The latter is recommended for prototyping because of the reduced cost; however, glass yields better signal transmission and detection. Additionally, glass fibers are strong but the fiber breaks with little stretching. Plastic fibers are cheap and more flexible than glass. However, they have much higher attenuation and a limited temperature range. Thus they are commonly used in designing sensor heads but once they are finalized, it is optimal to switch to glass. The size of the area of measurement will determine the fiber diameters both for sources and detectors. The placement of the sources and detectors for in-vivo measurements is highly dependent on the region of interest and based on the particular application. Proper understanding of photon propagation allows for an educated arrangement to come up with spatially resolved spectroscopy **(refer to Fig.2 (c))**. Illustrated are several modified configurations designed for the visual cortex from previous work (Kashou et al. 2007), **Fig. 7**. By varying the distance between the source and detectors we can manipulate the depth of the signal propagation. Optimizing the optode layout is highly dependent on the application and region of interest. The sensor heads with two detectors were designed to allow for the option of using only the inner sources, the outer sources or both simultaneously. The one detector sensor head was

designed to be more flexible by allowing the same option as the previous ones but with the addition of spatially varying the sensors (horizontally) and the detector (vertically) in order to manipulate the penetration depth of the signal.

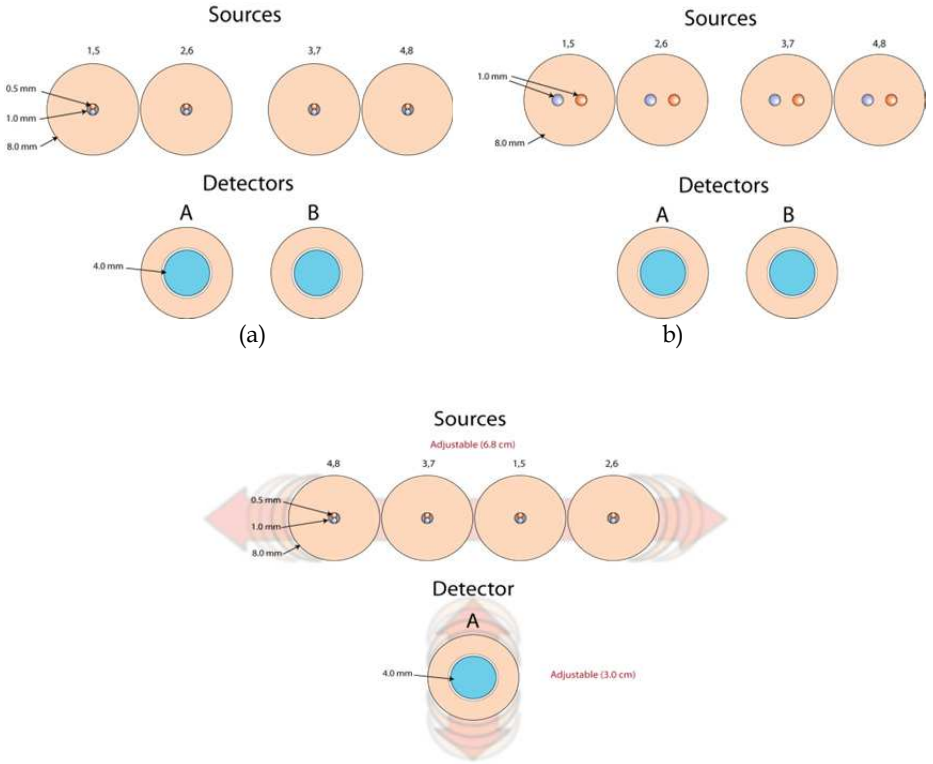

Fig. 7. Three optode layouts for visual cortex measurements using two wavelengths 690 (orange, sources 1-4) and 830 (gray, sources 5-8), transmitted through optical fibers and collected by the detector (s) (blue). (a) Co-located wavelengths with diameter of 0.5mm each and two detectors, (b) separated wavelengths with diameter of 1.0mm each and two detectors, (c) co-located wavelengths with diameter of 0.5mm each and one detector which are spatially adjustable.

Table 1, lists the approximate distances for the configurations illustrated in **Fig. 7 (a) & (c)**. Note, in configuration 1, the sensor head was not exactly symmetric and thus needs to be considered in the analysis of the signals. A more accurate methodology of fabrication and design of the sensor heads needs to be incorporated for the future as research labs move forward in this field. These numbers are important in the process of validating and optimizing the sensor head. They can also be used in the photon propagation simulation for correlation with experimental data. We will discuss simulation in detail in Section 3.

		Configuration 1		Configuration 2
Wavelength	Source	Distance from A	Distance from B	Minimum Distance from A
830 nm				
	1	3.2 cm	4.5 cm	2.0 cm
	2	3.0 cm	3.7 cm	2.5 cm
	3	3.7 cm	3.0 cm	2.0 cm
	4	4.8 cm	3.3 cm	2.5 cm
690 nm				
	5	3.2 cm	4.5 cm	2.0 cm
	6	3.0 cm	3.7 cm	2.5 cm
	7	3.7 cm	3.0 cm	2.0 cm
	8	4.8 cm	3.3 cm	2.5 cm

Table 1. The source detector distances from a one and two detector sensor head design for the visual cortex.

2.6 Optode configurations

In optical tomography, several approaches for optode configurations have been evaluated. Most of the clinical studies have been performed using two parallel glass plates which compress the tissue (such as the breast). This source-detector imaging configuration has the advantage to reduce the attenuation of the transmitted light through a well-known thickness of the interrogated structure. However, the compression technique induces changes in optical properties of the tissue (Gibson et al. 2005), and it is generally difficult to achieve depth resolution from off-axis transmission data acquired in parallel plane geometry. 3D image reconstruction can be ideally generated by surrounding the tissue with multiple sources and fibre-detectors. This circular configuration does not require compression, but the detected light intensities at the tissue boundaries notably decrease as the size of the tissue increases (Ntziachristos et al. 2002).

2.7 Applications

In this section, a more detailed look at the methods and techniques of selected studies is described, in order to gauge reader interest in the possibilities of future work. Since traditionally, imaging modalities in children usually involves higher risk and acceptance, NIR has and is proving to have potential in this population. As a result, new methods have been introduced for functional studies in infants with the hopes of carrying on to adults. An advantage of starting with infants is mainly because of anatomy and the distance the light has to traverse.

Single channel NIRS (Ferrari et al. 2004; Hoshi 2003; Obrig et al. 2000) has been used in the past to record brain activity. The typical design would have three possible photon paths. The first possible path is that the photon undergoes a number of scattering events to reach the detector. The second possibility is that the photon is absorbed after a number of scattering events. The third is that the photon leaves the head without being detected. Unfortunately, using a single channel NIRS technique has the major constraint of spatial resolution; hence multiple NIRS systems have been used for optical topography (Gratton et al. 1995). The first report of optical topography on premature babies included the use of nine sources and four detectors using a CW system (Chance et al. 1998). In a more recent study, optical topography in awake infants (Taga et al. 2003) was demonstrated by using the

Hitachi system. This multi-channel system used a CW source and generated two wavelengths (780 and 830*nm*). Twenty laser diodes and eight avalanche photodiode detectors were used and separated into individual light sources by 48 lock-in amplifiers. **Table 2** gives a non-exhaustive list of studies involving NIRS mainly for visual cortex monitoring.

Reference	Source	Detector	Wavelength	Type	Stimuli
Taga et al., 2003	20	8	780, 830	CW	Checkerboard
Wilcox et al., 2005		2	680, 830		Ball & Box
Chance et al., 1998	9	4		CW	
Toronov et al., 2000	16	2	758, 830	TD	
Franceschini et al., 2003	16	16	690, 830	CW	Finger tap
Franceschini et al., 2000	8	2	758, 830	FD	
Everdell et al., 2005	16	8	785, 850	FD	
Xu et al., 2005	9	4	808	CW	
Meek et al., 1995	4		779, 821, 855, 908	TD	Red, blue, green discs
Jasdzewski et al., 2003	2	4	682, 930	CW	Checkerboard
Plichta et al., 2006	17	16	695±20, 830±20	CW	Checkerboard
Wolf et al., 2003	4	2	670, 830	FD	Checkerboard
Gratton & Fabiani 2003	8	2	750	FD	Gratings (CP)
Schroeter et al., 2006a			775, 810, 850, 910		Checkerboard
Schroeter et al., 2004	8	7	780, 830	FD	Checkerboard
Miki et al., 2005			780, 805, 830		Monocular Flashes
Kusaka et al., 2004	8	8	776, 804, 828	CW	Flashing light
Obrig et al., 2000	4	1	775, 825, 850, 905		Checkerboard

Table 2. The details of the system and configurations used by some research groups.

3. Photon diffusion equation

We discussed MBLL earlier however a more efficient way of modeling and simulating the light path through tissue is by the photon diffusion equation. The well-known photon diffusion equation derived from the transport equation is widely used to describe photon migration in biological tissues:

$$\frac{1}{v}\frac{\partial}{\partial t}L(r,\vec{s},t)+\nabla.L(r,\vec{s},t).\vec{s}=-(\mu_a+\mu_S)L(r,\vec{s},t)+\mu_S\int_{4\pi}L(r,\vec{s}',t)P(\vec{s}',\vec{s})d\vec{s}'+S(r,\vec{s},t) \quad (11)$$

4. Photon simulation and reconstruction

4.1 Monte Carlo (MC) method

The 2D MC code proceeds in the following way: First, a photon packet is launched into the medium at the defined source position with an initial survival weight w that indicates the probability of a photon's successively propagation without absorption. Snell's law and Fresnel reflection formulas are then applied at each boundary. After each scattering event,

a new direction of the photon is determined using the Henyey-Greenstein scattering function. The effects of absorption in each region can be obtained by $exp(\mu_a L_m)$ where L_m is the partial path length of photon through region m. The survival weight and path length in each layer is recorded when the photon was scattered out of the head model, to obtain the photon trajectory.

The same rules used previously for the 2D MC code, to describe photon migration are also adopted for the 3D MC code. The tissue is divided into voxels, each of which may have different optical properties. In our simulation, before the photons started to emit, we created a matrix to record the spatial arrangement of tissue constituents. Each voxel in the matrix was assigned an integer to represent the type of tissue in the voxel. As the photon is propagated from one scattering event to the next, a check was made every 1 grid element of 1 mm spacing to see if the scattering or absorption coefficient has changed.

We performed 2D and 3D MC simulations based on various head models. We modified Monte Carlo code (Wang et al. 1995) to calculate the spatial sensitivity profiles *SSP* ("banana shaped"). The mean optical path length travelled by the detected light within each region m of the tissue types is defined as:

$$L_m = \frac{\partial \mathrm{A}}{\partial \mu_{\mathrm{a,m}}} \tag{12}$$

Where $A = -\ln(\mathrm{I}/I_0)$, which is the attenuation change in the detected intensity I and I_0 is the incident radiation. **Equation 13** can be used to calculate the radiation distribution profile (spatial sensitivity profile, SSP) which depends on the probability of photons traveling within a particular region m at position r from the source optode to the detector optode:

$$SSP(r) \equiv L_m(r) = \frac{\partial \mathrm{A}}{\partial \mu_{\mathrm{a,m}}(r)} \tag{13}$$

4.2 Head models

4.2.1 Two-dimensional head model

A three-layer semi-infinite slab having various scattering and absorption optical properties with the single optode spacings ρ = 28 mm, as shown in figure 1, is adopted. The layers start with the scalp-skull region of 7.9 mm, then the cerebrospinal fluid (CSF) of 1.5 mm and the brain being infinitely extended. The optical properties and thicknesses of each layer used for this model were chosen based on reports from literature.

4.2.2 Three-dimensional homogeneous head model

The sphere had dimensions of 40 x 40 x 40 mm with the single source optode positioned at (20,20,0) and 19 detectors depicted in **Fig. 8**, having each 1 mm of diameter, placed in various positions on the surface.

4.2.3 Three dimensional realistic head model

We used segmented MRI data (3D-SPGR, T1-weighted images) of an adult human head that we employed for 3D MC simulations. **Figure 8** shows the axial slice of the anatomical MRI, segmented into five tissue types (air, scalp, CSF, and gray/white matter). The whole volume

was contained within 512x512x120 voxels. The optical properties used for each tissue type were reported from literature. The source and detector were placed on the transaxial plane.

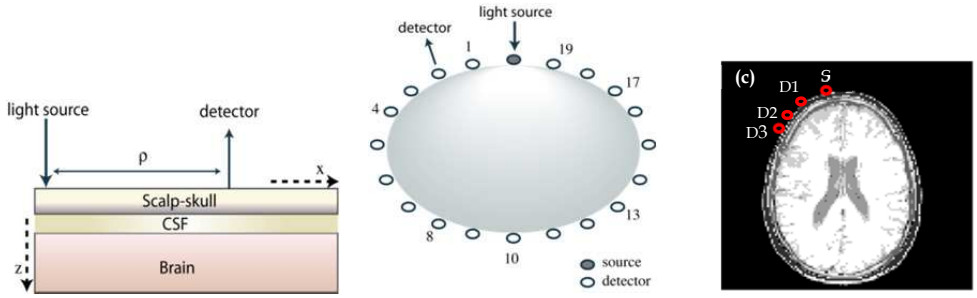

Fig. 8. (a) Two-dimensional heterogeneous, (b) Three-dimensional homogenous (symbols full and open circles indicate the position of the source and the detectors respectively) and (c) anatomical MRI, adult head models used in MC simulations (symbols S and D1-D3 indicate the position of the source and the detectors respectively).

5. Results and discussion

We simulated the radiation distribution so-called "banana-shape" in order to determine the contribution of the photons scattered from the different regions within the head model as function of separation distance between the source light and the detector location. We ran 10^8 photons for all MC simulations to achieve an appropriate SNR. The spatial sensitivity distributions were calculated for each head model. **Fig. 9** shows a cross section of the "banana shaped" across the 2D three-layer model **(Fig. 8(a))** for a source-detector separation of 28 mm, which is commonly used for NIRS. The effects of the CSF layer can clearly be seen as a significant reduction in the depth penetration of light. The ratio of photons scattering through the brain decreases, such that most of the light is detected from scalp-skull layer. A significant part of photons was guided along the CSF layer, which has the effect of concentrating measurement sensitivity to the more superficial layer (scalp-skull) and may change the depth sensitivity profile.

The sensitivity measurements at various source-detector spacings **(Fig. 9)** was investigated by considering a 3D homogeneous head model **(Fig. 8 (b))**. The migrating of all 10^8 photons was performed in a single 3D MC simulation for all 19 detectors at same time. The sensitivity to deeper region seems to vary between different source-detector spacings, as shown in figures **(Fig. 10 (a)-(d))**. For the smaller optode spacings, the minimum depth is obtained **Fig. 10(a)-(b)**. As the separation between the source and the detector increases, the depth of penetration by the detected light also increases but intensity of light decreases more strongly, as shown in **Fig. 10 (c)-(d)**. This model can be useful in investigating the propagation of light in the infant brain. A reference homogeneous phantom (Hebden et al. 2002) was previously used in representing the premature infant brain which consisted of a balloon filled in a solution of intralipid.

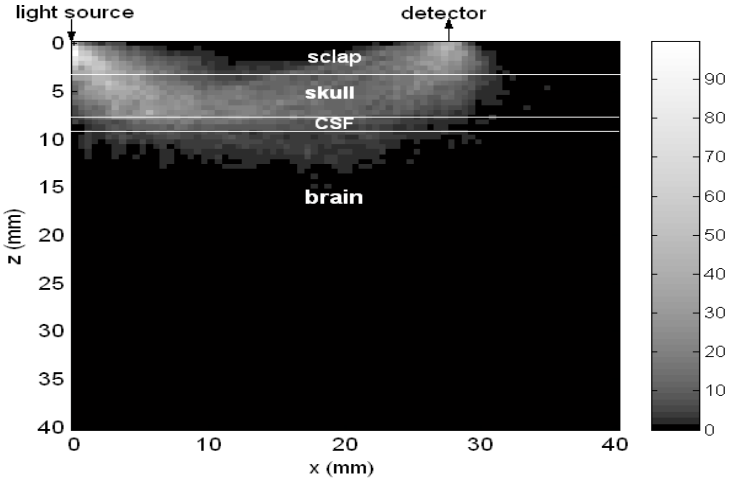

Fig. 9. Spatial sensitivity profile of photons in 2D three-layer head model as given by MC simulation for a single source- detector separation. Light in the near-infrared range (700-900 nm), compared to the visible light range penetrates tissues more deeply. The photons change direction multiples times as they scatter, and they follow a generally curved path called the "banana shaped" curve between the light source and the detector location at the surface (Mansouri and L'Huillier, 2007).

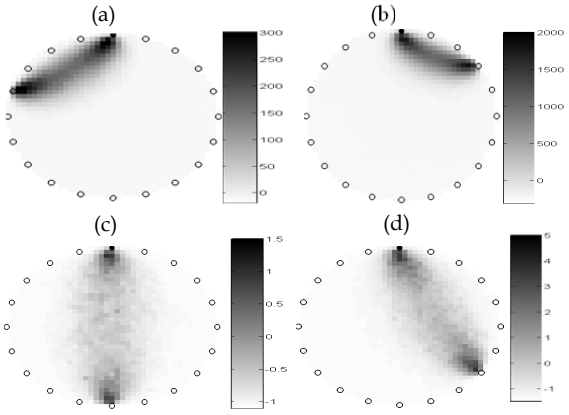

Fig. 10. ("banana shaped") photon distributions through the homogeneous 3D head model between the single source and various detectors 4, 17,10, and 13 from (a) to (d) respectively.

Fig. 11 shows a cross section of the "banana shaped" across the 3D segmented MR image **(Fig. 8 (c))**. The light penetration between the source and the detector is not along any major gray matter, however, a significant part of the light is detected from scalp and skull. This suggests that the contribution of light that travels within the superficial layers of the scalp and skull to the whole detected light is rather large. This indicates that the number of photons that travel through the brain surface are the largest among the detected photons penetrating into the brain tissue which spreads near the brain surface. Thus, the

fundamental question that arises here: is the NIR signal sensitive to changes associated with functional brain activation? While NIRS is increasingly gaining attention in studies on brain function, the sensitivity of NIRS signals to functional brain activation remains to be discussed.

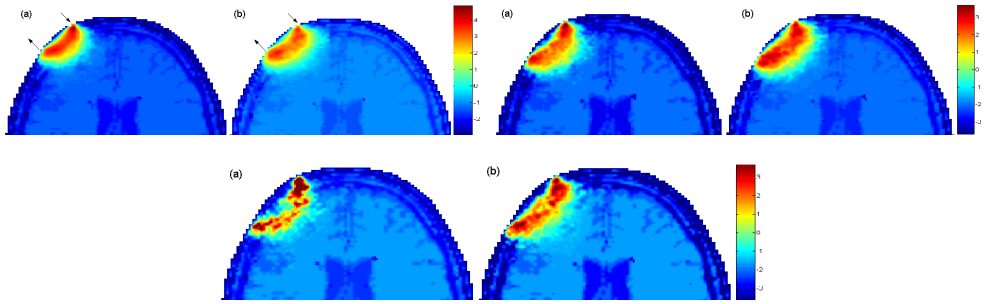

Fig. 11. Spatial sensitivity profiles of photons in the realistic 3D head model. Depth sensitivity is limited by the presence of endogenous chromophores such as haemoglobin, water and cytochrome. The optical path travelled by photons between the source and the detector is strongly dependent to the thickness and the optical properties of the superficial tissues and the 'void' region, which is the CSF of the head. Data measurements from multiple source-detector separations provide overlapping measurement from a limited area. These are used for tomographic image reconstruction utilising 3D models (Mansouri et al., 2010).

The present study has demonstrated that the path length is strongly dependent on the thickness and the optical properties of the superficial tissues and the CSF in the head model. This indicates that the contribution of the extracerebral layers to the radiation distribution is large, while the contribution of the brain is small. Therefore, the estimation of the optical path travelled by photons between the source and the detector is crucial for evaluating the sensitivity of NIRS signals to the brain.

6. Conclusion

In this chapter, we presented a technical overview of NIRS as it relates to the medical field. NIRS has the potential to be the wide spread standard of care in hospitals. Mainly because it is low cost, non-invasive, and portable. The number of research groups both preclinical and clinical using this technology is on the rise. This is because the nature of the light propagation and the depth of penetration of NIRS is ideal for the infant population. As seen in this chapter, there is still room for improvement and even though not discussed here, there are studies trying to measure neuronal responses using NIRS. Other groups have tried to combine NIRS with various modalities. There are still challenges which are being tackled, such as sensor head design and optimization. However, within the next several years it is expected that there will be much more advancement to this promising modality.

7. References

Arridge, S. R. (1995). "Photon-measurement density functions. Part I: Analytical forms." *Appl Opt* 34(31): 7395-7409.

Arridge, S. R. and W. R. Lionheart (1998). "Nonuniqueness in diffusion-based optical tomography." *Opt Lett* 23(11): 882-884.

Arridge, S. R. and M. Schweiger (1995). "Photon-measurement density functions. Part 2: Finite-element-method calculations." *Appl Opt* 34(34): 8026-8037.

Benaron, D. A., S. R. Hintz, et al. (2000). "Noninvasive functional imaging of human brain using light." *Journal of Cerebral Blood Flow and Metabolism* 20(3): 469-477.

Benaron, D. A. and D. K. Stevenson (1993). "Optical time-of-flight and absorbance imaging of biologic media." *Science* 259(5100): 1463-1466.

Boas, D. A., M. A. Franceschini, et al. (2002). Noninvasive Imaging of Cerebral Activation with Diffuse Optical Tomography, *In vivo optical imaging optical imaging of brain function*. R. D. Frostig, CRC Press.

Brazy, J. E., D. V. Lewis, et al. (1985). "Noninvasive Monitoring of Cerebral Oxygenation in Preterm Infants - Preliminary-Observations." *Pediatrics* 75(2): 217-225.

Chance, B., E. Anday, et al. (1998). "A novel method for fast imaging of brain function, non-invasively, with light." *Optics Express* 2(10): 411-423.

Chance, B., J. S. Leigh, et al. (1988). "Comparison of Time-Resolved and Time-Unresolved Measurements of Deoxyhemoglobin in Brain." *Proceedings of the National Academy of Sciences of the United States of America* 85(14): 4971-4975.

Cope, M. (1991). The Application of Near-Infrared Spectroscopy to Non Invasive Monitoring of Cerebral Oxygenation in the Newborn Infant. *Department of Medical Physics and Bioengineering*. London, University College London. PhD.

Cope, M. and D. T. Delpy (1988). "System for Long-Term Measurement of Cerebral Blood and Tissue Oxygenation on Newborn-Infants by near-Infrared Trans-Illumination." *Medical & Biological Engineering & Computing* 26(3): 289-294.

Cubeddu, R., A. Pifferi, et al. (1996). "Time-resolved imaging on a realistic tissue phantom: mu(s)' and mu(a) images versus time-integrated images." *Appl Opt* 35(22): 4533-4540.

Everdell, N. L., A. P. Gibson, et al. (2005). "A frequency multiplexed near-infrared topography system for imaging functional activation in the brain." *Review of Scientific Instruments* 76(9): -.

Ferrari, M., L. Mottola, et al. (2004). "Principles, techniques, and limitations of near infrared spectroscopy." *Canadian Journal of Applied Physiology-Revue Canadienne De Physiologie Appliquee* 29(4): 463-487.

Franceschini, M. A., S. Fantini, et al. (2003). "Hemodynamic evoked response of the sensorimotor cortex measured noninvasively with near-infrared optical imaging." *Psychophysiology* 40(4): 548-560.

Franceschini, M. A., V. Toronov, et al. (2000). "On-line optical imaging of the human brain with 160-ms temporal resolution." *Optics Express* 6(3): 49-57.

Gandjbakhche, A. H., R. Nossal, et al. (1994). "Resolution Limits for Optical Transillumination of Abnormalities Deeply Embedded in Tissues." *Medical Physics* 21(2): 185-191.

Gibson, A. P., J. C. Hebden, et al. (2005). "Recent advances in diffuse optical imaging." *Physics in Medicine and Biology* 50(4): R1-R43.

Gratton, E., S. Fantini, et al. (1997). "Measurements of scattering and absorption changes in muscle and brain." *Philosophical Transactions of the Royal Society of London Series B-Biological Sciences* 352(1354): 727-735.

Gratton, G., P. M. Corballis, et al. (1995). "Shades of Gray-Matter - Noninvasive Optical-Images of Human Brain Responses during Visual-Stimulation." *Psychophysiology* 32(5): 505-509.

Gratton, G. and M. Fabiani (2003). "The event-related optical signal (EROS) in visual cortex: Replicability, consistency, localization, and resolution." *Psychophysiology* 40(4): 561-571.

Greisen, G. (2006). "Is near-infrared spectroscopy living up to its promises?" *Seminars in Fetal & Neonatal Medicine* 11(6): 498-502.

Grosenick, D., H. Wabnitz, et al. (1997). "Time-resolved imaging of solid phantoms for optical mammography." *Applied Optics* 36(1): 221-231.

Hebden, J. C., S. R. Arridge, et al. (1997). "Optical imaging in medicine: I. Experimental techniques." *Physics in Medicine and Biology* 42(5): 825-840.

Hebden, J. C., A. Gibson, et al. (2002). "Three-dimensional optical tomography of the premature infant brain." *Physics in Medicine and Biology* 47(23): 4155-4166.

Hintz, S. R., D. A. Benaron, et al. (2001). "Bedside functional imaging of the premature infant brain during passive motor activation." *Journal of Perinatal Medicine* 29(4): 335-343.

Hintz, S. R., D. A. Benaron, et al. (1998). "Stationary headband for clinical time-of-flight optical imaging at the bedside." *Photochemistry and Photobiology* 68(3): 361-369.

Hintz, S. R., W. F. Cheong, et al. (1999). "Bedside imaging of intracranial hemorrhage in the neonate using light: Comparison with ultrasound, computed tomography, and magnetic resonance imaging." *Pediatric Research* 45(1): 54-59.

Hoshi, Y. (2003). "Functional near-infrared optical imaging: Utility and limitations in human brain mapping." *Psychophysiology* 40(4): 511-520.

Jasdzewski, G., G. Strangman, et al. (2003). "Differences in the hemodynamic response to event-related motor and visual paradigms as measured by near-infrared spectroscopy." *Neuroimage* 20(1): 479-488.

Jiang, H., K. D. Paulsen, et al. (1995). "Simultaneous reconstruction of optical absorption and scattering maps in turbid media from near-infrared frequency-domain data." *Opt Lett* 20(20): 2128-2130.

Kashou, N. H., R. Xu, et al. (2007). "Using FMRI and FNIRS for localization and monitoring of visual cortex activities." *Conf Proc IEEE Eng Med Biol Soc* 2007: 2634-2638.

Kato, T., A. Kamei, et al. (1993). "Human visual cortical function during photic stimulation monitoring by means of near-infrared spectroscopy." *J Cereb Blood Flow Metab* 13(3): 516-520.

Kennan, R. P., S. G. Horovitz, et al. (2002). "Simultaneous recording of event-related auditory oddball response using transcranial near infrared optical topography and surface EEG." *Neuroimage* 16(3): 587-592.

Kusaka, T., K. Kawada, et al. (2004). "Noninvasive optical Imaging in the visual cortex in young infants." *Human Brain Mapping* 22(2): 122-132.

Maki, A., Y. Yamashita, et al. (1996). "Visualizing human motor activity by using non-invasive optical topography." *Front Med Biol Eng* 7(4): 285-297.

Mansouri, C. and J. P. L'Huillier (2007). "Time-resolved photon migration through an adult head model: Comparison between Finite Element and Monte Carlo calculations -

art. no. 66320L." *Therapeutic Laser Applications and Laser-Tissue Interaction III* 6632: L6320-L6323.

Mansouri, C., J. P. L'Huillier, et al. (2010). "Depth sensitivity analysis of functional near-infrared spectroscopy measurement using three-dimensional Monte Carlo modelling-based magnetic resonance imaging." *Lasers in Medical Science* 25(3): 431-438.

Meek, J. H., C. E. Elwell, et al. (1995). "Regional Changes in Cerebral Hemodynamics as a Result of a Visual Stimulus Measured by near-Infrared Spectroscopy." *Proceedings of the Royal Society of London Series B-Biological Sciences* 261(1362): 351-356.

Meek, J. H., M. Firbank, et al. (1998). "Regional hemodynamic responses to visual stimulation in awake infants." *Pediatric Research* 43(6): 840-843.

Miki, A., T. Nakajima, et al. (2005). "Near-infrared spectroscopy of the visual cortex in unilateral optic neuritis." *American Journal of Ophthalmology* 139(2): 353-356.

Nioka, S., Q. Luo, et al. (1997). "Human brain functional imaging with reflectance CWS." *Oxygen Transport to Tissue Xix* 428: 237-242.

Ntziachristos, V., J. Ripoll, et al. (2002). "Would near-infrared fluorescence signals propagate through large human organs for clinical studies? (vol 27, pg 333, 2002)." *Optics Letters* 27(18): 1652-1652.

Obrig, H. and A. Villringer (2003). "Beyond the visible - Imaging the human brain with light." *Journal of Cerebral Blood Flow and Metabolism* 23(1): 1-18.

Obrig, H., R. Wenzel, et al. (2000). "Near-infrared spectroscopy: does it function in functional activation studies of the adult brain?" *International Journal of Psychophysiology* 35(2-3): 125-142.

Plichta, M. M., M. J. Herrmann, et al. (2006). "Event-related functional near-infrared spectroscopy (fNIRS): Are the measurements reliable?" *Neuroimage* 31(1): 116-124.

Pogue, B., M. Testorf, et al. (1997). "Instrumentation and design of a frequency-domain diffuse optical tomography imager for breast cancer detection." *Optics Express* 1(13): 391-403.

Pogue, B. W. and M. S. Patterson (1994). "Frequency-Domain Optical-Absorption Spectroscopy of Finite Tissue Volumes Using Diffusion-Theory." *Physics in Medicine and Biology* 39(7): 1157-1180.

Pouratian, N., S. A. Sheth, et al. (2003). "Shedding light on brain mapping: advances in human optical imaging." *Trends Neurosci* 26(5): 277-282.

Schroeter, M. L., M. M. Bucheler, et al. (2004). "Towards a standard analysis for functional near-infrared imaging." *Neuroimage* 21(1): 283-290.

Schroeter, M. L., M. M. Bucheler, et al. (2006a). "Circadian variability is negligible in primary visual cortices as measured by fNIRS." *International Journal of Psychophysiology* 62(1): 9-13.

Schroeter, M. L., T. Kupka, et al. (2006b). "Investigating the post-stimulus undershoot of the BOLD signal - A simultaneous fMRI and fNIRS study." *Neuroimage* 30(2): 349-358.

Siegel, A., J. J. Marota, et al. (1999). "Design and evaluation of a continuous-wave diffuse optical tomography system." *Optics Express* 4(8): 287-298.

Strangman, G., D. A. Boas, et al. (2002). "Non-invasive neuroimaging using near-infrared light." *Biological Psychiatry* 52(7): 679-693.

Strangman, G., M. A. Franceschini, et al. (2003). "Factors affecting the accuracy of near-infrared spectroscopy concentration calculations for focal changes in oxygenation parameters." *Neuroimage* 18(4): 865-879.

Taga, G., K. Asakawa, et al. (2003). "Brain imaging in awake infants by near-infrared optical topography." *Proceedings of the National Academy of Sciences of the United States of America* 100(19): 10722-10727.

Toronov, V., M. A. Franceschini, et al. (2000). "Near-infrared study of fluctuations in cerebral hemodynamics during rest and motor stimulation: Temporal analysis and spatial mapping." *Medical Physics* 27(4): 801-815.

Villringer, A. and B. Chance (1997). "Non-invasive optical spectroscopy and imaging of human brain function." *Trends in Neurosciences* 20(10): 435-442.

Wang, L., S. L. Jacques, et al. (1995). "MCML--Monte Carlo modeling of light transport in multi-layered tissues." *Computer Methods and Programs in Biomedicine* 47(2): 131-146.

Wilcox, T., H. Bortfeld, et al. (2005). "Using near-infrared spectroscopy to assess neural activation during object processing in infants." *Journal of Biomedical Optics* 10(1): -.

Wolf, M., U. Wolf, et al. (2003). "Fast cerebral functional signal in the 100-ms range detected in the visual cortex by frequency-domain near-infrared spectrophotometry." *Psychophysiology* 40(4): 521-528.

Wyatt, J. S., M. Cope, et al. (1988). "The Response of Cerebral Blood-Volume to Changes in Arterial Carbon-Dioxide Tension Measured by near-Infrared Spectroscopy in Newborn-Infants." *Early Human Development* 17(2-3): 291-291.

Xu, C., D. Wang, et al. (2005). "Continuous-wave Near-infrared Topography System and Its Clinical Application." *Conf Proc IEEE Eng Med Biol Soc* 1: 196-198.

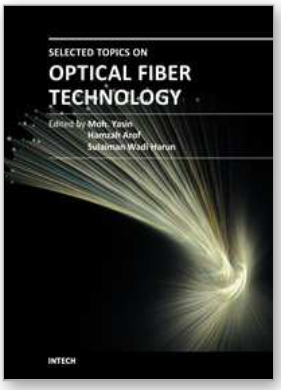

Selected Topics on Optical Fiber Technology

Edited by Dr Moh. Yasin

ISBN 978-953-51-0091-1
Hard cover, 668 pages
Publisher InTech
Published online 22, February, 2012
Published in print edition February, 2012

This book presents a comprehensive account of the recent advances and research in optical fiber technology. It covers a broad spectrum of topics in special areas of optical fiber technology. The book highlights the development of fiber lasers, optical fiber applications in medical, imaging, spectroscopy and measurement, new optical fibers and sensors. This is an essential reference for researchers working in optical fiber researches and for industrial users who need to be aware of current developments in fiber lasers, sensors and other optical fiber applications.

INTECH
open science | open minds

InTech Europe
University Campus STeP Ri
Slavka Krautzeka 83/A
51000 Rijeka, Croatia
Phone: +385 (51) 770 447
Fax: +385 (51) 686 166
www.intechopen.com

InTech China
Unit 405, Office Block, Hotel Equatorial Shanghai
No.65, Yan An Road (West), Shanghai, 200040, China
中国上海市延安西路65号上海国际贵都大饭店办公楼405单元
Phone: +86-21-62489820
Fax: +86-21-62489821